The Astrophysical Journal, 721:622–629, 2010 September 20 doi:10.1088/0004-637X/721/1/622

MAGNETIC NON-POTENTIALITY OF SOLAR ACTIVE REGIONS AND PEAK X-RAY FLUX OF THE ASSOCIATED FLARES

Sanjiv Kumar Tiwari, P. Venkatakrishnan, and Sanjay Gosain
Udaipur Solar Observatory, Physical Research Laboratory, Dewali, Bari Road, Udaipur 313 001, India; pvk@prl.res.in, sgosain@prl.res.in
Received 2010 March 15; accepted 2010 July 27; published 2010 August 31

ABSTRACT

Predicting the severity of solar eruptive phenomena such as flares and coronal mass ejections remains a great challenge despite concerted efforts to do so over the past several decades. However, the advent of high-quality vector magnetograms obtained from *Hinode* (SOT/SP) has increased the possibility of meeting this challenge. In particular, the spatially averaged signed shear angle (SASSA) seems to be a unique parameter for quantifying the non-potentiality of active regions. We demonstrate the usefulness of the SASSA for predicting flare severity. For this purpose, we present case studies of the evolution of magnetic non-potentiality using 115 vector magnetograms of four active regions, namely, ARs NOAA 10930, 10960, 10961, and 10963 during 2006 December 8–15, 2007 June 3–10, 2007 June 28–July 5, and 2007 July 10–17, respectively. The NOAA ARs 10930 and 10960 were very active and produced X and M class flares, respectively, along with many smaller X-ray flares. On the other hand, the NOAA ARs 10961 and 10963 were relatively less active and produced only very small (mostly A- and B-class) flares. For this study, we have used a large number of high-resolution vector magnetograms obtained from *Hinode* (SOT/SP). Our analysis shows that the peak X-ray flux of the most intense solar flare emanating from the active regions depends on the magnitude of the SASSA at the time of the flare. This finding of the existence of a lower limit of the SASSA for a given class of X-ray flares will be very useful for space weather forecasting. We have also studied another non-potentiality parameter called the mean weighted shear angle (MWSA) of the vector magnetograms along with the SASSA. We find that the MWSA does not show such distinction as the SASSA for upper limits of the *GOES* X-ray flux of solar flares; however, both the quantities show similar trends during the evolution of all active regions studied.

Key words: Sun: flares – Sun: surface magnetism – sunspots

Online-only material: color figures

1. INTRODUCTION

Many magnetic parameters, e.g., twist, shear, and energy, computed for complex active regions have been examined with a view to predicting the severity of solar eruptive phenomena such as flares and coronal mass ejections (CMEs). Although such studies have been carried out for several decades, the progress remains slow. Here, we study two of these parameters, i.e., magnetic non-potentiality inferred from the spatially averaged signed shear angle (SASSA) and the mean weighted shear angle (MWSA) of sunspots.

Magnetic shears at polarity inversion lines were studied previously to look for flare-related changes (e.g., Hagyard et al. 1984, 1990; Ambastha et al. 1993; Hagyard et al. 1999). The magnetic energy change following a few flares has been estimated by Schrijver et al. (2008) and Jing et al. (2010). Jing et al. (2010) found that the magnitudes of free magnetic energy were different for the flare-active and the flare-quiet regions, but the temporal variation of free magnetic energy did not show any clear and consistent pre-flare pattern. A study of the evolution of global alpha (α_g) for one highly eruptive and one quiet-active region has been performed by Tiwari (2009), but no correlation between α_g and the *GOES* X-ray flux was found. Sudol & Harvey (2005) found changes in the line-of-sight magnetic field associated with flares. The unsigned flux of NOAA AR 10930 has been studied recently by Abramenko et al. (2008). Figure 2 of Abramenko et al. (2008) shows that the unsigned net flux of NOAA AR 10930 does not show any relationship with the peak *GOES* X-ray flux.

Despite many such attempts, the severity of flares has not been successfully predicted. In this paper, we make an effort to determine an upper limit of the peak X-ray flux of solar flares emanating from active regions as a function of the magnitude of the SASSA and the MWSA. These parameters, namely, SASSA and MWSA, give a quantitative measure of the non-potentiality present in an active region at an observed height. More details about the SASSA and the MWSA are given in Section 2.

Many researchers have used the force-free parameter α as a measure of the magnetic twist of the sunspots. Many forms of global α have been proposed and studied such as $\alpha_{\rm best}$ (Pevtsov et al. 1995), α_{av} (Hagino & Sakurai 2004), and α_g (Tiwari et al. 2009a, 2009b; Tiwari 2009). The force-free parameter α actually gives twice the degree of twist per unit axial length along the axis of the flux rope (see Appendix A of Tiwari et al. 2009a). Thus, α provides the gradient of twist at a certain observational height and not the actual twist of an active region. The signs of the global α (α_g) and the SASSA are found to be similar but the magnitudes are not correlated (Tiwari et al. 2009b). Recently, α_g has been studied for the time series of two active regions, NOAA AR 10930 and 10961, by Tiwari (2009), as mentioned earlier. The global α does not show any clear indication of predicting the severity of X-ray flares. The reason could be due to the non-validity of the linear force-free assumption for such complex active regions. The local and global α values of several active regions were studied by Hahn et al. (2005), Nandy et al. (2003), and Nandy (2008). They found that the global α ($\alpha_{\rm best}$) was not important for the flare activity. However, they noticed a decrease in the variance of spatial α distribution after the flare.

To explore the utility of the SASSA as a predictor of flare severity, we have studied the evolution of SASSA in a time series of vector magnetograms of two highly flare productive sunspots, i.e., NOAA ARs 10930 and 10960, and also two

less flare productive sunspots, i.e., NOAA ARs 10961 and 10963. The AR 10930 has been the most active sunspot observed by *Hinode* (SOT/SP). Three major X-class flares, i.e., X6.5, X3.4, and X1.5, were observed by *Hinode* (SOT/SP) on 2006 December 6, 13, and 14, respectively. Many C- and B-class flares were also associated with the same sunspot. Similarly NOAA AR 10960 was also highly flare productive and produced four M-class flares. On the other hand, the NOAA ARs 10961 and 10963 were relatively less flare productive.

The main purpose of this study is to find the lower limit of the non-potentiality parameters, if any, for a given class of X-ray flares.

In Section 2, we briefly describe the magnetic parameters SASSA and MWSA. In Section 3, we give details of the data sets used. Section 4 illustrates the analysis and results obtained. Finally, in Section 5 we discuss the results and present our conclusions.

2. THE MAGNETIC NON-POTENTIAL PARAMETERS USED IN THIS STUDY

2.1. Spatially Averaged Signed Shear Angle

The signed shear angle (SSA) represents the deviation of observed transverse vectors from potential transverse vectors with a positive or a negative sign. It has a sign similar to the photospheric chirality of sunspots (Tiwari 2009; Tiwari et al. 2009b). The SSA is computed from the following formula:

$$\mathrm{SSA} = \tan^{-1}\left(\frac{B_{yo}B_{xp} - B_{yp}B_{xo}}{B_{xo}B_{xp} + B_{yo}B_{yp}}\right), \quad (1)$$

where B_{xo}, B_{yo} and B_{xp}, B_{yp} are the observed and potential transverse components of sunspot magnetic fields, respectively.

The SASSA is taken to quantify the global non-potentiality of the whole sunspot. This parameter gives the non-potentiality of a sunspot irrespective of the force-free nature (Tiwari et al. 2009b) and shape of the sunspot (Venkatakrishnan & Tiwari 2009). Thus, the SASSA is a very important magnetic parameter for quantifying the non-potentiality of any active region.

Apart from measuring the non-potentiality, the SASSA also retains the sign of chirality of the active region magnetic field, unlike other shear parameters such as the MWSA. This property of sign seems to be crucial to obtaining the proper measure of global non-potentiality, as will be explained later in this paper.

2.2. Mean Weighted Shear Angle

The MWSA was introduced by Wang (1992) to quantitatively study the changes in magnetic structure and the build-up of the magnetic shear. The MWSA is given as

$$\mathrm{MWSA} = \frac{\sum |B_t|\theta}{\sum |B_t|}, \quad (2)$$

where B_t is the measured transverse field strength and θ is the difference between the observed and potential azimuths. The potential fields have been computed by taking the longitudinal field as a boundary. The method used in computing the potential field is as per Sakurai (1989).

The reason for calculating the weighted mean instead of a simple average of the shear angle is that the MWSA filters the weak field area. The stronger fields play a more important role in determining the field structure and can be measured more accurately. We should note here that the MWSA will weight more on the high transverse field regions like penumbral fields, a fact that will be shown later in this paper to explain the relatively lower success of the MWSA as a flare intensity predictor.

3. DATA SETS USED

We have used the series of vector magnetograms of two eruptive ARs, NOAA 10930 and 10960, and two less eruptive ARs, NOAA 10961 and 10963, obtained from the Solar Optical Telescope/Spectro-polarimeter (SOT/SP; Tsuneta et al. 2008; Suematsu et al. 2008; Ichimoto et al. 2008; Shimizu et al. 2008) on board *Hinode* (Kosugi et al. 2007).

The *Hinode* (SOT/SP) data have been calibrated by the standard "SP_PREP" routine developed by B. Lites and is available in the Solar-Soft package. The prepared polarization spectra have been inverted to obtain vector magnetic field components using an Unno–Rachkowsky (Unno 1956; Rachkowsky 1967) inversion under the assumption of the Milne–Eddington atmosphere (Landolfi & Landi Degl'Innocenti 1982; Skumanich & Lites 1987). We use the "STOKESFIT" inversion code which is available in the Solar-Soft package and was developed by T. R. Metcalf. The latest version of the inversion code is used which returns the true field strengths along with the filling factor.

There is an inherent 180° ambiguity in the azimuth determination due to the insensitivity of the Zeeman effect to the sense of orientation of the transverse magnetic fields. Numerous techniques have been developed and applied to resolve this problem (for details see Metcalf et al. 2006; Leka et al. 2009), but a complete resolution is not expected from the physics of the Zeeman effect. The chirality of chromospheric and coronal structures can be used as guides to complement the other methods. The 180° azimuthal ambiguity in our data sets has been removed by using the acute angle method (Harvey 1969; Sakurai et al. 1985; Cuperman et al. 1992). This method of ambiguity resolution works very well for magnetic shear angles that are less than 90°. Less than 1% of pixels of any vector magnetogram studied have a shear of ∼90°. Therefore, we expect that the acute angle method works well in all of our cases. Most of the data sets used have a spatial sampling of ∼0.3 arcsec pixel^{-1}. A few data sets are observed in "Normal Mode" of the SOT with a spatial sampling of ∼0.16 arcsec pixel^{-1}.

The noise in the data has been minimized similar to the method used in Tiwari (2009), Tiwari et al. (2009b), and Venkatakrishnan & Tiwari (2009, 2010). This method is as follows: only the pixels having transverse (B_t) and longitudinal magnetic field (B_z) values greater than a certain level are analyzed. To determine this critical threshold, a quiet Sun region is selected for each active region and the 1σ deviation in the three vector field components B_x, B_y, and B_z is evaluated separately. The resultant 1σ deviation in B_x and B_y is then taken as the noise level for transverse field components. Only those pixels with longitudinal and transverse fields simultaneously greater than twice the above-mentioned noise levels are analyzed.

To minimize the projection effects, the magnetograms are transformed into the heliographic coordinates wherever they are more than 10° away from the disk center (Venkatakrishnan et al. 1988; Venkatakrishnan & Gary 1989).

Information about different classes of X-ray flares is collected from the Web sites http://www.solarmonitor.org/index.php and http://www.spaceweather.com/. We have also used the *GOES* X-ray data.

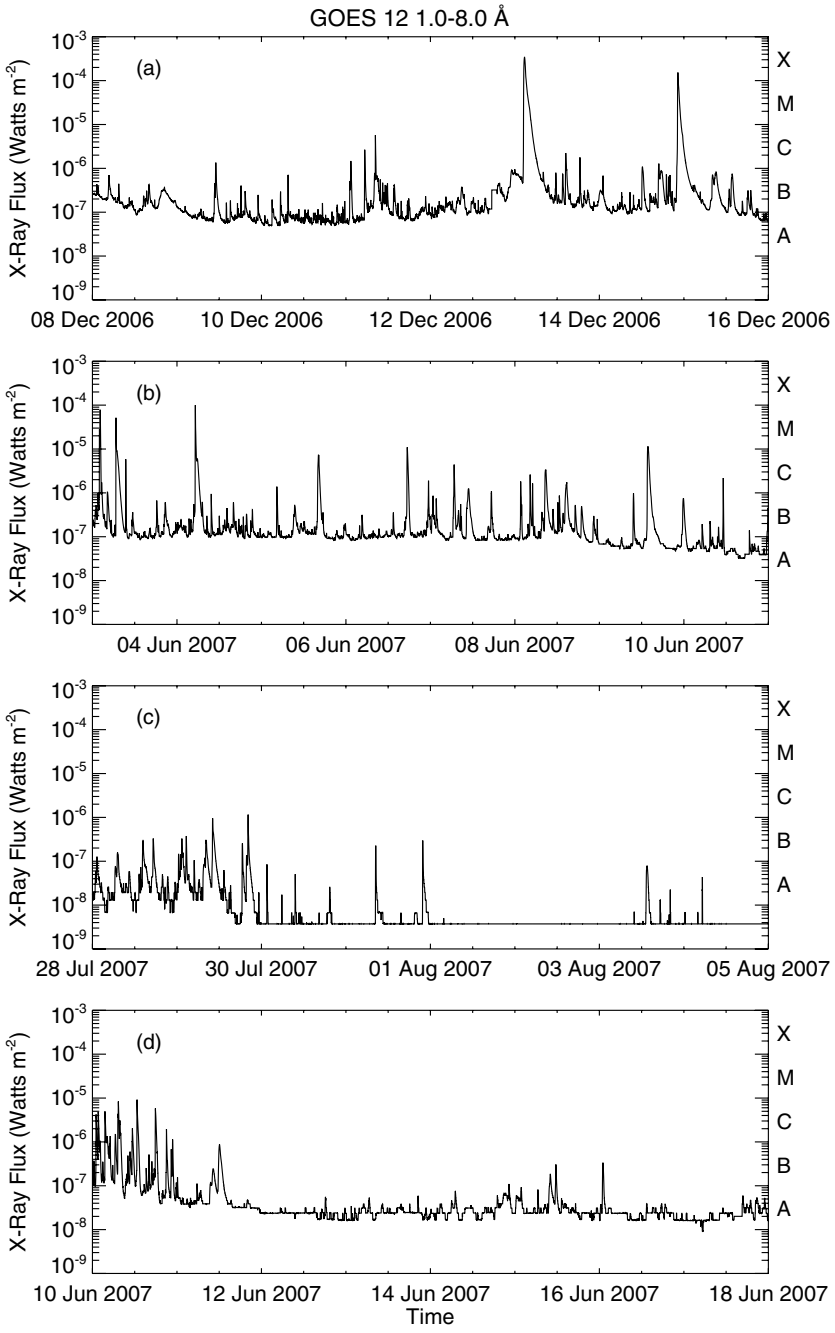

Figure 1. Time variation plots of the X-ray flux from the *GOES* 12 satellite in the wavelength range 1–8 Å. (a) The data ranges from 2006 December 9 to 2006 December 15 when the highly active NOAA AR 10930 was present on the solar disk. Two X-class and many C- and B-class flares occurred. (b) Four M-class flares and several C- and B-class flares were observed in NOAA AR 10960. (c) and (d) Both panels show less activity, with mostly B- and A-class flares in NOAA ARs 10961 and 10963, respectively.

4. DATA ANALYSIS AND RESULTS

Figure 1 shows *GOES* 12 X-ray plots (in the wavelength range 1.0–8.0 Å) of different X-ray flares observed during the disk passage of NOAA ARs 10930, 10960, 10961, and 10963. We see that the *GOES* X-ray peaks show high activity with two X-class flares and several C-class flares during 2006 December 8–15 in NOAA AR 10930 (Figure 1(a)). High activity is also seen with four M-class and several C-class flares during 2007 June 3–10 through the disk passage of NOAA AR 10960 (Figure 1(b)). The *GOES* X-ray light curves show less activity with very small B- and A-class flares during 2007 June 28−July 5 in NOAA AR 10961 (Figure 1(c)). Figure 1(d) also presents a weak activity with some C-class flares in the beginning but mostly B- and A-class flares in later evolution stages of NOAA AR 10963 during 2007 July 10–18.

A large number of vector magnetograms of eruptive NOAA ARs 10930 (36) and 10960 (21) have been analyzed. Also, 28 and 30 vector magnetograms of the less eruptive NOAA ARs 10961 and 10963, respectively, are analyzed to study the evolution of these sunspot magnetic fields. One longitudinal image with the transverse vectors of each active region has been shown in Figure 2. The red and blue contours represent the positive and negative fields of ±1000, ±1500, and ± 3000 G.

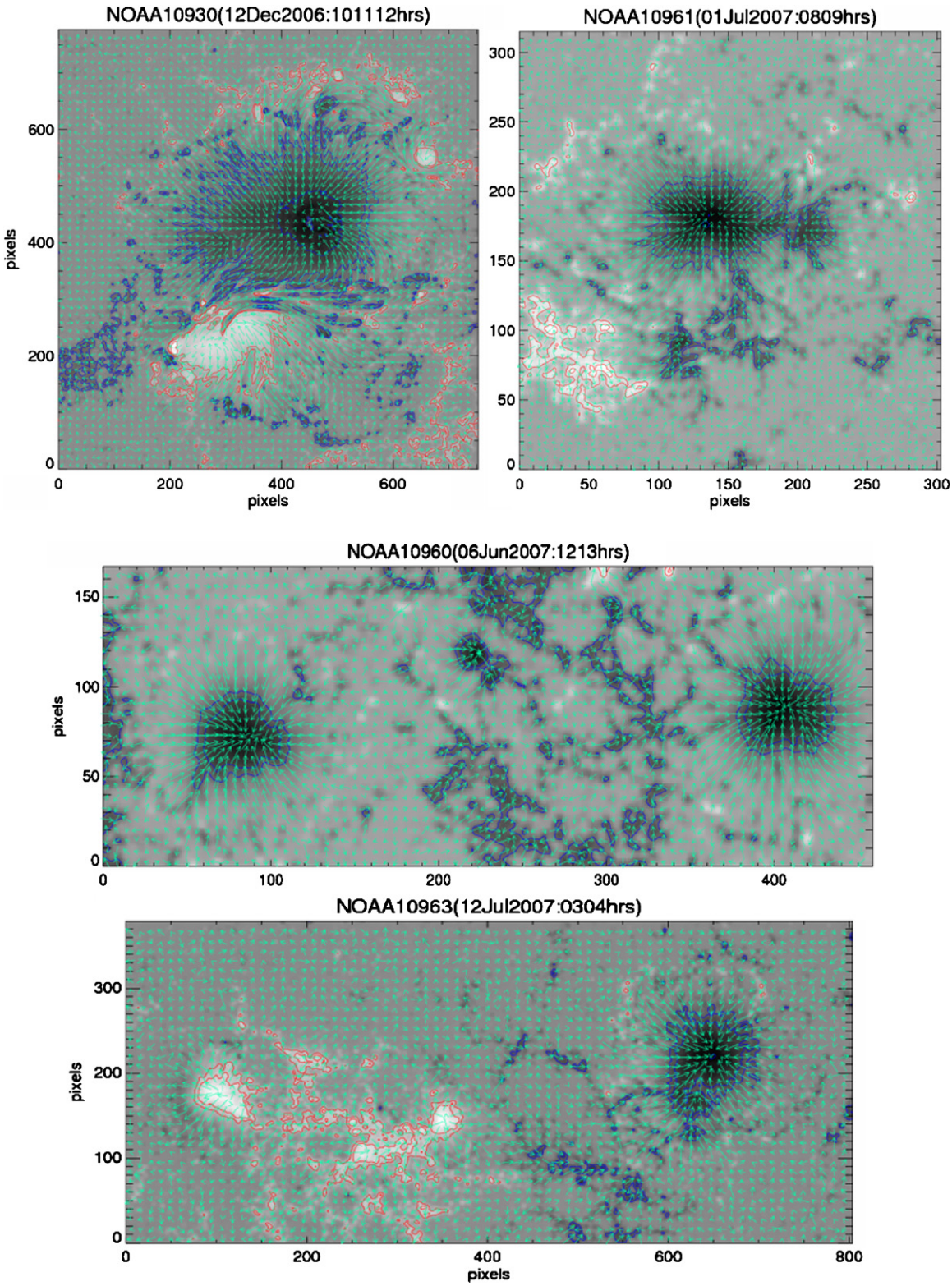

Figure 2. Examples of one longitudinal image with the transverse vectors of each active region studied are shown. The red and blue contours represent the positive and negative fields of ±1000, ±1500, and ± 3000 G.

(A color version of this figure is available in the online journal.)

4.1. Temporal Evolution of the SASSA and the MWSA

Figures 3 and 4 show the plots of the SASSA and the MWSA in highly active regions NOAA ARs 10930 and 10960 and the relatively quiet NOAA ARs 10961 and 10963, respectively. The diamonds and stars represent the SASSA and the MWSA, respectively. The dotted/dashed vertical lines show the time and class of flares associated with these active regions. The lines with big red dashes in Figure 3(a) represent the timings of X-class flares. The orange dash-dotted lines in Figure 3(b)

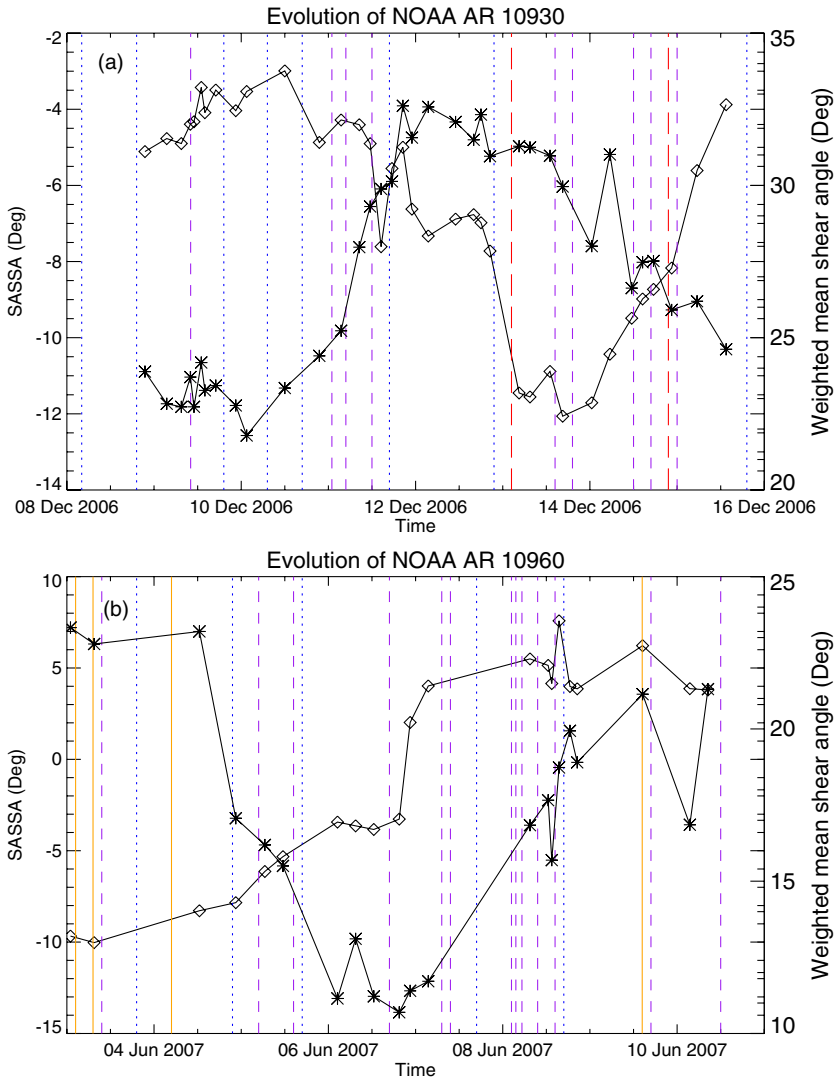

Figure 3. Evolution of the SASSA and MWSA in NOAA ARs 10930 and 10960 is shown. The boxes and stars represent the SASSA and the MWSA, respectively. (a) The red big dashed vertical lines represent timings of two X-class flares. Purple smaller dashed lines show the timings of C-class flares and blue dotted lines represent the timings of B-class flares. (b) The orange dash-dotted lines show the timings of M-class flares. The dashed purple and dotted blue lines again show the timings of C- and B-class flares as above.

(A color version of this figure is available in the online journal.)

show the timings of M-class flares. The lines with small purple dashes in all figures represent the timings of C-class flares. The blue dotted lines in Figures 3(a) and 3(b) represent the timings of B-class flares. The black dotted lines in Figures 4(a) and 4(b) represent the timings of A-class flares whereas the blue dashed lines in these figures represent the timings of B-class flares.

4.1.1. Evolution of the SASSA and the MWSA in NOAA AR 10930

From the plots of the SASSA in Figure 3(a), it can be clearly seen that any X-class flare occurred only when the SASSA was greater than 8°. If the SASSA was greater than 4°, then C-class flares also occurred. If the SASSA was less than 4°, only B-class flares happened. It should be noted that the sign of the SASSA with magnitudes is given in the figures only to express the sense of chirality of non-potentiality. Similarly, the MWSA was greater than 26° and 22° for X- and C-class flares, respectively. B-class flares occurred if the MWSA was greater than 21°.

We can notice that both of the non-potentiality parameters show a similar trend during the evolution period of the active region. However, the threshold values of the MWSA for C- and B-class flares are very close.

4.1.2. Evolution of the SASSA and the MWSA in NOAA AR 10960

Figure 3(b) shows that the M-class flares took place when the SASSA exceeded 6°. The M-class flares did not occur whenever the SASSA was less than 6°. One interesting behavior that can be seen during the evolution of this active region is the chirality inversion. In the beginning, the SASSA is highly negative and three M-class flares took place. The SASSA started decreasing, allowing only three C-class flares and became positive by building up non-potentiality again. As the SASSA became more than 4°, C-class flares again started taking place. After seven C-class flares, one M-class flare took place when the SASSA exceeded 6°. Even in this peculiar evolution of the active region, the SASSA maintained its upper limits for different classes of X-ray flares as observed in the NOAA AR 10930. Thus, we see a symmetrical behavior of the threshold values, independent of the sign of the SASSA.

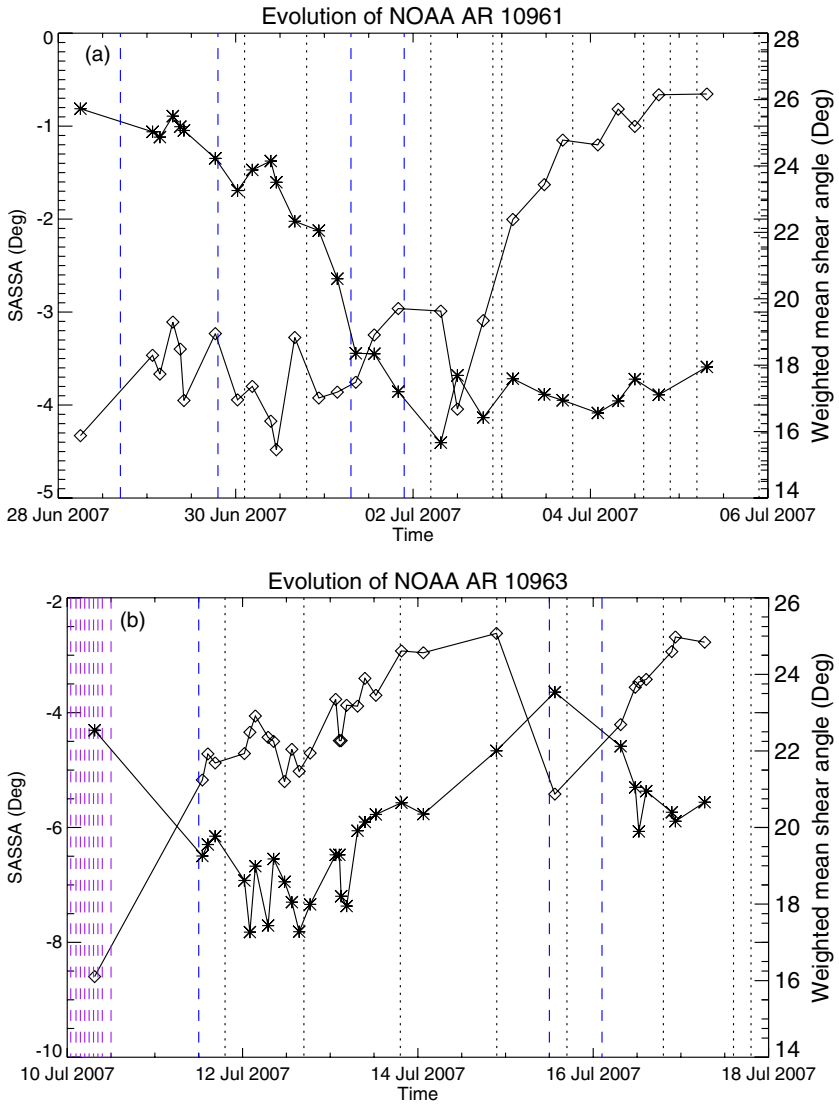

Figure 4. Evolution of the SASSA in NOAA AR 10961 and NOAA AR 10963. Both are relatively quiet regions. The boxes and stars represent the SASSA and the MWSA, respectively. (a) The blue dashed vertical lines represent the timings of B-class X-ray flares and the black dotted lines represent the timings of A-class flares. (b) The purple dashed lines show timings of C-class flares. The blue dashes and black dots represent timings of B- and A-class flares, respectively.

(A color version of this figure is available in the online journal.)

The MWSA shows a behavior almost similar to the SASSA. The MWSA was high in the beginning, started decreasing after some flares had taken place, and built up again, showing a trend similar to the SASSA. It can be noted, however, that for C-class flares, the MWSA stays very small up to 11° and could not maintain its upper limit as decided in the case of NOAA AR 10930. The MWSA values observed for M-class flares are seen to be more than 22° which matches up with those of the C-class flares observed in NOAA AR 10930. Thus, the threshold values of the MWSA seem to be specific to the active region, and thus seem to be of dubious utility for flare intensity prediction.

4.1.3. Evolution of the SASSA and the MWSA in NOAA AR 10961

The NOAA AR 10961 is the quietest active region out of the four studied. Only B- and A-class flares occurred during the disk passage of this active region, as can be seen in Figure 4(a). From Figure 4(a), one can see that the B-class flares occurred in NOAA AR 10961 when the SASSA was greater than ∼2.°5. Only small A-class flares took place when the SASSA was less than 2°.

The MWSA had to be greater than 16° and 14°, respectively, for any B- and A-class flares to occur. The MWSA shows a trend very similar to the SASSA, but the threshold values again seem to be specific to the active regions.

4.1.4. Evolution of the SASSA and the MWSA in NOAA AR 10963

The NOAA AR 10963 is relatively quieter than the first two active regions, NOAA ARs 10930 and 10960. It produced several C-class flares in the beginning of the observations and later became very quiet, triggering only B- and A-class flares as shown in Figure 4(b). From Figure 4(b), we note that the SASSA was high on July 10 when several consecutive C-class flares took place. No C-class flare took place when the SASSA became less than 4°, complementing the behavior seen in the cases of Figures 3(a) and 3(b). No B-class flare occurred when the SASSA was less than 2.°5 as observed in Figure 4(a). Thus, the SASSA maintains its threshold values even for very small flares.

The MWSA was observed greater than 20° for C-class flares. For every B- and A-class flare, the MWSA was greater than 18° and 16°, respectively. The MWSA again shows a similar

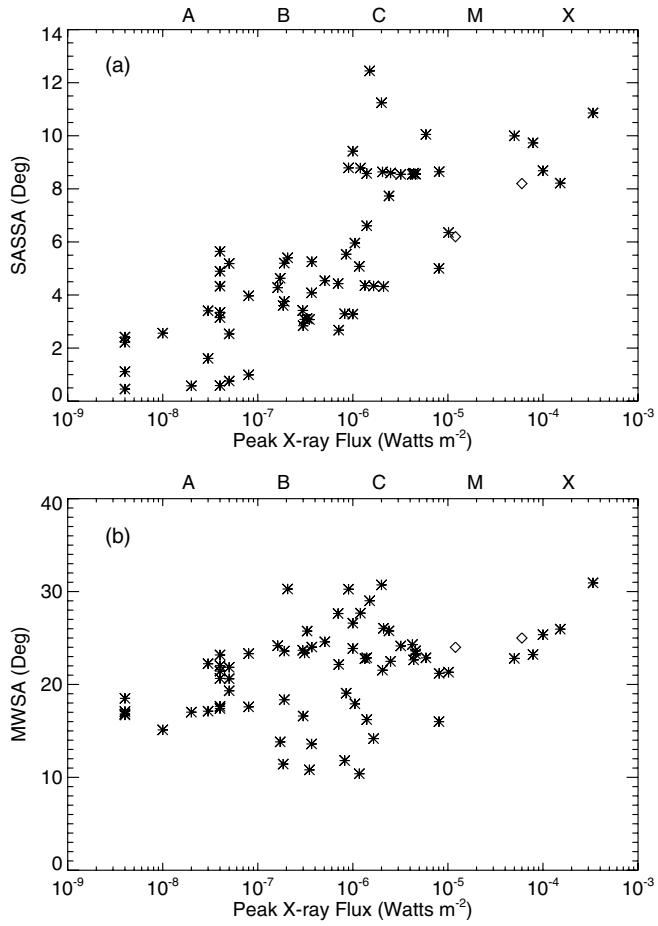

Figure 5. (a) Scatter plot between the SASSA and peak X-ray flux of the *GOES* 12 satellite. Samples include all the events associated with all four active regions, i.e., NOAA ARs 10930, 10960, 10961, and 10963. The magnitude of the SASSA at the time of the peak X-ray flux has been interpolated from the available sample of the SASSA, as shown in Figures 3 and 4. Also, the approximate values of the SASSA corresponding to M-class flares in two cases have been taken from Table 1 of Tiwari et al. (2009b) and are shown by diamond symbols. (b) The same as panel (a), except for values of the MWSA instead of the SASSA.

evolutionary behavior to that of the SASSA. The threshold values, however, were specific to the active region.

Thus, we conclude that the SASSA can be used as a reliable predictor of the maximum possible flux of X-ray flares. The data for studying the evolution of the SASSA in more active regions are not available at present. However, the inspection of the different flares which occurred in all the sunspots listed in Table 1 of Tiwari et al. (2009b) shows a similar trend. From Table 1 of Tiwari et al. (2009b), we also confirm a threshold value of $\sim 6^\circ$ for M-class flares as shown in our Figure 3(b). The peak fluxes of M-class flares associated with NOAA AR 10808 and NOAA AR 09591 are shown with their SASSA and MWSA values, respectively, by diamond symbols in Figures 5(a) and 5(b).

4.2. Statistical Relation between the Peak X-ray Flux and the Non-potentiality Parameters

Figures 5(a) and 5(b) represent scatter plots between the peak *GOES* X-ray flux and interpolated SASSA and MWSA values for that time, respectively. The cubic spline interpolation of the sample of the SASSA and the MWSA values has been done to get the SASSA and the MWSA exactly at the time of peak flux of the X-ray flare.

4.2.1. Statistical Relation between the Peak X-ray Flux and the SASSA

From Figure 5(a), it can be noted that there is a good relationship between the minimum value of the magnitude of the SASSA and the observed value of the peak *GOES* X-ray flux. Thus, a lower limit of the SASSA can be assigned to each class of X-ray flares.

4.2.2. Statistical Relation between the Peak X-ray Flux and the MWSA

Figure 5(b) (for the values of the MWSA) does not show as good of a correlation with the peak X-ray flux as the SASSA shows. The MWSA is small even for higher classes of flares. One possible reason for such behavior of the MWSA is explained in Section 5.

5. DISCUSSION AND CONCLUSIONS

From Figures 3 and 4, it is very clear that an upper limit of the peak X-ray flux for a given value of the SASSA can be given for different classes of X-ray flares. Thus, we conclude that the SASSA, apart from its helicity sign-related studies, can also be used to predict the severity of the solar flares. However, to establish these lower limits of the SASSA for different classes of X-ray flares, we need more cases to study. The SASSA has already given a good indication of its utility from the present four case studies using 115 vector magnetograms from *Hinode* (SOT/SP). Once the vector magnetograms are routinely available with higher cadence, the lower limit of the SASSA for each class of X-ray flares can be established by calculating the SASSA in a series of vector magnetograms. This will provide input for space weather models.

The other non-potentiality parameter studied in this paper, the MWSA, does show a similar trend to that of the SASSA. The magnitudes of the MWSA, however, do not show consistent threshold values in relation to the peak *GOES* X-ray flux of different classes of solar flares. One possible reason for this behavior may be explained as follows: the MWSA weights the strong transverse fields, e.g., penumbral fields. From recent studies (Su et al. 2009; Tiwari et al. 2009b; Tiwari 2009; Venkatakrishnan & Tiwari 2009, 2010), it is clear that the penumbral field contains complicated structures with opposite signs of vertical current and vertical component of the magnetic tension forces. Although the amplitudes of the magnetic parameters are found high in the penumbra, they do not contribute to their global values because they contain opposite signs, which cancel out in the averaging process (Tiwari 2009; Tiwari et al. 2009b). On the other hand, the MWSA adds those high values of the shear and produces a pedestal that might mask any relation between the more relevant global non-potentiality and the peak X-ray flux whereas the SASSA perhaps gives a more relevant value of the shear after the cancellation of the penumbral contribution.

The other parameters such as the unsigned net flux and global alpha (α_g) do not show a good correlation with the *GOES* X-ray flux as discussed in Section 1. However, the evolution of the SASSA in 10930 during 2006 December 9–14 shows a good correlation with the free magnetic energy, as seen in Figure 6 of Jing et al. (2010). In particular, the SASSA remains about 5° during 2006 December 9–11 and increases up to about 12° by the end of 2006 December 13. The free magnetic energy (as computed by Jing et al. 2010) follows a similar trend with

values of about 40×10^{31} erg during 2006 December 9–11 which increase up to 90×10^{31} erg by 2006 December 14. Thus, the SASSA seems to be a good indicator of free magnetic energy as well.

We now proceed to give a plausible reason for the success of the SASSA as a predictor of maximum flare intensity. Basically, we need two ingredients for a flare. We need available magnetic energy (non-potential field energy) and we also need a flare trigger which is usually magnetic reconnection driven by the flux emergence. A flare cannot occur in the absence of either ingredient. However, in the present study, we find that a single global property of the spot, namely, the SASSA, determines the class of a flare, if one were to occur. The flare class, as classified by soft X-ray emission, indicates the maximum amount of X-ray emission and therefore maximum mass of the emitting plasma. Our definition of the SASSA is basically an indication of the amount of non-potentiality in the field configuration. It has already been established that higher non-potentiality is related to lower magnetic tension (Venkatakrishnan 1990; Venkatakrishnan et al. 1993). Further, lower magnetic tension implies larger scale heights of the magnetic pressure for a force-free field. A larger scale height of magnetic pressure means a more extended field, and thus a larger volume of emitting gas filling these extended fields by chromospheric evaporation during a flare. A larger volume of emitted plasma results in higher X-ray emission for typical densities of the evaporated plasma. This explanation can be tested by detailed modeling or by observing flares at the solar limb for sunspots with known amounts of the SASSA or on the disk using stereoscopic observations. If this explanation is indeed borne out by such studies, then it will confirm the importance of the SASSA for the dynamical equilibrium of sunspots.

The peak X-ray emission of flares was also found to be correlated with the initial speed of the associated CME (Ravindra 2004). The initial speed of CMEs was in turn found to be related to the severity of the geomagnetic storm (Srivastava & Venkatakrishnan 2002). Thus, the SASSA might also turn out to be a good parameter for predicting the severity of geomagnetic storms. This will be investigated in future research.

Other parameters, such as free magnetic energy and tension forces, can also be studied to examine the pre-flare equilibrium configuration of a flaring active region. All these quantities, once studied together in a large number of cases, will certainly provide a better prediction of flare severity. Monitoring the evolution of the SASSA and other magnetic parameters will require high-cadence vector magnetograms which can be obtained from filter-based instruments such as the Solar Vector Magnetograph (Gosain et al. 2004, 2006, 2008), the Multi-Application Solar Telescope (Venkatakrishnan 2006) from the ground, and the Helioseismic and Magnetic Imager (Scherrer & SDO/HMI Team 2002) aboard the *SDO*, from the space.

We thank the referee for very useful comments which improved the manuscript. The authors acknowledge IFCPAR (Indo-French Centre for Promotion of Advanced Research) for financial support. We acknowledge SWPC for providing *GOES* X-ray data. *Hinode* is a Japanese mission developed and launched by ISAS/JAXA, collaborating with NAOJ as a domestic partner and NASA and STFC (UK) as international partners. Scientific operation of the *Hinode* mission is conducted by the *Hinode* science team organized at ISAS/JAXA. This team mainly consists of scientists from institutes in the partner countries. Support for the post-launch operation is provided by JAXA and NAOJ (Japan), STFC (UK), NASA (USA), and ESA and NSC (Norway).

REFERENCES

Abramenko, V., Yurchyshyn, V., & Wang, H. 2008, ApJ, 681, 1669
Ambastha, A., Hagyard, M. J., & West, E. A. 1993, Sol. Phys., 148, 277
Cuperman, S., Li, J., & Semel, M. 1992, A&A, 265, 296
Gosain, S., Tiwari, S. K., Joshi, J., & Venkatakrishnan, P. 2008, J. Astrophys. Astron., 29, 107
Gosain, S., Venkatakrishnan, P., & Venugopalan, K. 2004, Exp. Astron., 18, 31
Gosain, S., Venkatakrishnan, P., & Venugopalan, K. 2006, J. Astrophys. Astron., 27, 285
Hagino, M., & Sakurai, T. 2004, PASJ, 56, 831
Hagyard, M. J., Stark, B. A., & Venkatakrishnan, P. 1999, Sol. Phys., 184, 133
Hagyard, M. J., Teuber, D., West, E. A., & Smith, J. B. 1984, Sol. Phys., 91, 115
Hagyard, M. J., Venkatakrishnan, P., & Smith, J. B., Jr. 1990, ApJS, 73, 159
Hahn, M., Gaard, S., Jibben, P., Canfield, R. C., & Nandy, D. 2005, ApJ, 629, 1135
Harvey, J. W. 1969, PhD thesis, Univ. of Colorado, Boulder
Ichimoto, K., et al. 2008, Sol. Phys., 249, 233
Jing, J., Tan, C., Yuan, Y., Wang, B., Wiegelmann, T., Xu, Y., & Wang, H. 2010, ApJ, 713, 440
Kosugi, T., et al. 2007, Sol. Phys., 243, 3
Landolfi, M., & Landi Degl'Innocenti, E. 1982, Sol. Phys., 78, 355
Leka, K. D., Barnes, G., Crouch, A. D., Metcalf, T. R., Gary, G. A., Jing, J., & Liu, Y. 2009, Sol. Phys., 260, 83
Metcalf, T. R., et al. 2006, Sol. Phys., 237, 267
Nandy, D. 2008, in ASP Conf. Ser. 383, Subsurface and Atmospheric Influences on Solar Activity, ed. R. Howe et al. (San Francisco, CA: ASP), 201
Nandy, D., Hahn, M., Canfield, R. C., & Longcope, D. W. 2003, ApJ, 597, L73
Pevtsov, A. A., Canfield, R. C., & Metcalf, T. R. 1995, ApJ, 440, L109
Rachkowsky, D. N. 1967, Izv. Krym. Astrofiz. Obs., 37, 56
Ravindra, B. 2004, PhD thesis, Bangalore Univ.
Sakurai, T. 1989, Space Sci. Rev., 51, 11
Sakurai, T., Makita, M., & Shibasaki, K. 1985, MPA Rep. 212 (Garching: MPA), 312
Scherrer, P. H., & SDO/HMI Team 2002, BAAS, 34, 735
Schrijver, C. J., et al. 2008, ApJ, 675, 1637
Shimizu, T., et al. 2008, Sol. Phys., 249, 221
Skumanich, A., & Lites, B. W. 1987, ApJ, 322, 473
Srivastava, N., & Venkatakrishnan, P. 2002, Geophys. Res. Lett., 29, 090000
Su, J. T., Sakurai, T., Suematsu, Y., Hagino, M., & Liu, Y. 2009, ApJ, 697, L103
Sudol, J. J., & Harvey, J. W. 2005, ApJ, 635, 647
Suematsu, Y., et al. 2008, Sol. Phys., 249, 197
Tiwari, S. K. 2009, PhD thesis, Mohanlal Sukhadia Univ.
Tiwari, S. K., Venkatakrishnan, P., Gosain, S., & Joshi, J. 2009a, ApJ, 700, 199
Tiwari, S. K., Venkatakrishnan, P., & Sankarasubramanian, K. 2009b, ApJ, 702, L133
Tsuneta, S., et al. 2008, Sol. Phys., 249, 167
Unno, W. 1956, PASJ, 8, 108
Venkatakrishnan, P. 1990, Sol. Phys., 128, 371
Venkatakrishnan, P. 2006, in 2nd UN/NASA Workshop on International Heliophysical Year and Basic Space Science, Abstract Book, 33
Venkatakrishnan, P., & Gary, G. A. 1989, Sol. Phys., 120, 235
Venkatakrishnan, P., Hagyard, M. J., & Hathaway, D. H. 1988, Sol. Phys., 115, 125
Venkatakrishnan, P., Narayanan, R. S., & Prasad, N. D. N. 1993, Sol. Phys., 144, 315
Venkatakrishnan, P., & Tiwari, S. K. 2009, ApJ, 706, L114
Venkatakrishnan, P., & Tiwari, S. K. 2010, A&A, 516, L5
Wang, H. 1992, Sol. Phys., 140, 85